

Short Note

N-(1-Deoxy- α -D-tagatopyranos-1-yl)-*N*-methylaniline ("D-Tagatose-*N*-methylaniline")

Valeri V. Mossine ^{1,*} , Charles L. Barnes ² and Thomas P. Mawhinney ¹

¹ Department of Biochemistry, University of Missouri, Columbia, MO 65211, USA; mawhinneyt@missouri.edu

² Department of Chemistry, University of Missouri, Columbia, MO 65211, USA; BarnesCh@missouri.edu

* Correspondence: mossinev@missouri.edu; Tel.: +1-573-882-2608

Received: 17 April 2018; Accepted: 7 May 2018; Published: 9 May 2018



Abstract: Tagatosamines form in thermally-processed dairy products and contribute to the foods' organoleptic and nutritional value. *D*-Tagatose-*N*-methylaniline (*N*-(1-deoxy-*D*-tagatos-1-yl)-*N*-methylaniline, 1-deoxy-1-(*N*-methylphenylamino)-*D*-tagatose) was synthesized from *D*-galactose via the Amadori rearrangement. In aqueous solution, it established an anomeric equilibrium consisting of 62.8% α -pyranose, 21.3% β -pyranose, 1.5% α -furanose, 8.1% β -furanose, and 6.2% acyclic *keto* tautomer. The crystalline α -pyranose anomer of *D*-tagatose-*N*-methylaniline adopted the ⁵C₂ chair conformation. All hydroxyl and ring oxygen atoms and the amino nitrogen are involved in an extensive H-bonding network dominated by infinite homodromic chains. The Hirshfeld surface analysis suggests a significant contribution of non-polar intermolecular contacts to the crystal structure.

Keywords: carbohydrate; amino sugar; 1-deoxy-1-(*N*-methylphenylamino)-*D*-tagatose; tagatosamine; Amadori compound; tautomerization; crystal structure; Hirshfeld surface

1. Introduction

Tagatosamine is a common name for *N*-substituted 1-amino-1-deoxy-tagatose derivatives which belong to a diverse group of early Maillard reaction intermediates that form non-enzymatically in biological systems and in foods. In heated milk, lactose undergoes partial hydrolysis with release of free *D*-galactose and *D*-glucose. Under elevated temperatures, dehydration, or prolonged storage conditions, these reducing sugars can react with free amino groups of amino acids and proteins to form glycosylamines which, in turn, undergo the Amadori rearrangement to form lactulosamines, *D*-tagatosamines, and *D*-fructosamines, along with many polymeric and volatile products of the Maillard reaction [1–3]. In food sciences, the Maillard reaction is recognized as one of the main chemical transformations of food carbohydrates responsible for the characteristic aromas, color and nutritional value of pasteurized, baked, or roasted foods [4], but it is also a potential health hazard [5]. Consequently, there is a significant interest in 1-amino-1-deoxy-*D*-tagatose structure, reactivity, and biological activity, due to its presence in processed dairy foods and formulas. In addition, the ability of synthetic *D*-tagatosamine derivatives to disrupt the aggregation of tumor cells in cancer metastasis models [6] suggests that a therapeutic potential for this class of compounds needs to be investigated.

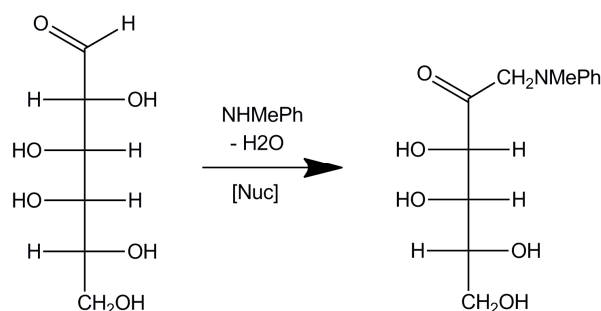
Nevertheless, in comparison to an extensive fructosamine research base [7], tagatosamines have been characterized sparsely [8,9]. Only two *N*-substituted 1-amino-1-deoxy-*D*-tagatose structures [10,11] have been solved by diffraction methods, so far. As part of our program on development of antimetastatic carbohydrate-based agents [12], we prepared a tagatosamine derivative of an aromatic amine, *D*-tagatose-*N*-methylaniline (1-deoxy-1-(*N*-methylphenylamino)-*D*-tagatose,

N-(1-deoxy-D-tagatos-1-yl)-*N*-methylaniline). We report here an analysis of its NMR and X-ray diffraction data and a Hirshfeld surface analysis of the molecules in the crystal.

2. Results and Discussion

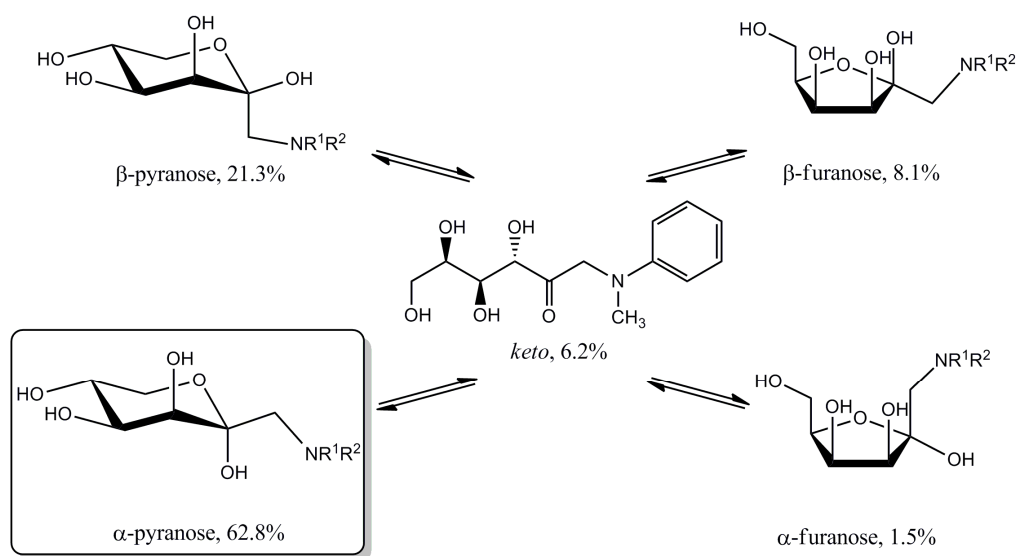
2.1. Chemistry and Structure Description

D-Tagatose-*N*-methylaniline was prepared from D-galactose and *N*-methylaniline in one step, following a conventional Amadori rearrangement protocol [13] (Scheme 1).



Scheme 1. Synthesis of D-tagatose-*N*-methylaniline from D-galactose.

In aqueous solution, the compound establishes an equilibrium (Scheme 2), with the α -pyranose being a predominant anomeric form, followed by the β -pyranose, β -furanose, and α -furanose anomers, as would be expected for a tagatose derivative (Table 1). The predominance of α -D-tagatopyranose is expected since the pyranoid structure is preferred for reducing carbohydrates in water, while the equatorial disposition of the hydroxyl groups and the anomeric effect favor the α -anomer [14]. However, there is a notable (6.2%) proportion of the acyclic keto tautomer. Previously reported estimates for the population of the acyclic forms of tagatose or tagatosamines in aqueous solutions did not exceed 0.8% (Table 1). On the other hand, enhanced formation of the acyclic carbohydrate forms was observed in D-fructosamine derivatives with hydrophobic amino substituents that are in close proximity to the carbonyl group, and this phenomenon was attributed to the localized hydrophobic effects around the carbonyl group [13,15]. A similar, albeit smaller, effect was reported for 1-deoxy-tagatose (Table 1), as well.



Scheme 2. Tautomeric equilibrium in aqueous solution of D-tagatose-*N*-methylaniline.

Table 1. Tentative assignments of chemical shifts (ppm) in ^{13}C -NMR spectra and percentage of D-tagatose-*N*-methylaniline (D-TagNMa) tautomers in 1:1 pyridine/ D_2O and in solid state at 25 °C. For comparison, the tautomeric compositions of D-tagatose [8,16], 1-deoxy-D-tagatose [17,18], D-tagatose-L-proline [8], and D-fructose-*N*-methylaniline (D-FruNMa) [13] are given.

Carbon	α -Pyranose	β -Pyranose	α -Furanose	β -Furanose	Acyclic Keto	Crystalline State
C-1	61.95	61.00	59.84	58.80	62.68	62.7
C-2	101.57	102.63	108.10	106.63	213.84	97.61
C-3	74.21	72.24	79.16	74.42	76.62	71.50
C-4	74.87	74.14	73.90	73.64	74.1	72.78
C-5	69.22	67.39	81.64	82.30	73.06	69.12
C-6	65.20	62.40	62.6	62.40	65.30	62.7
% for D-TagNMa	62.8	21.3	1.5	8.1	6.2	100 α -pyr
% for D-Tag	78.4	14.6	1.8	4.7	0.5	100 α -pyr
% for 1-deoxy-D-Tag	75	19	2	2	2	100 α -pyr
% for D-Tag-L-Pro	70.2	19.4	5.6	4.1	0.8	-
% for D-FruNMa	2.3	51.2	4.6	31.9	10.1	100 acyclic

D-Tagatose-*N*-methylaniline crystallized exclusively in the α -pyranose form, as evidenced by solid-state ^{13}C -NMR data (Table 1, Figure 1) and the following X-ray diffraction study.

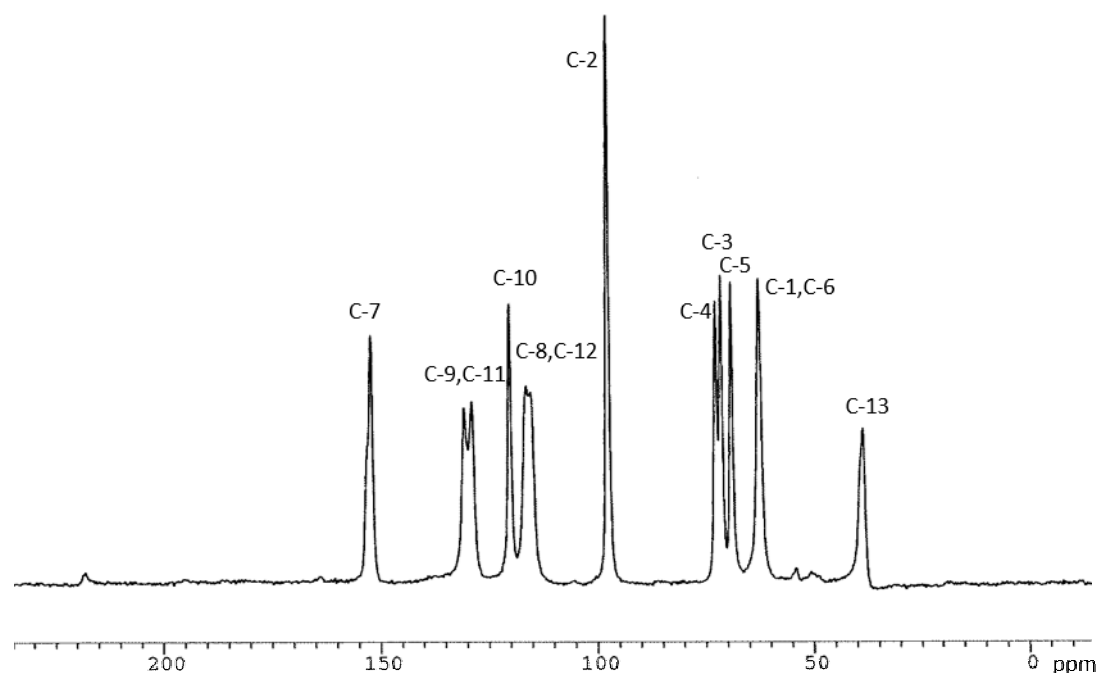


Figure 1. A solid-state ^{13}C -NMR spectrum of crystalline D-tagatose-*N*-methylaniline.

2.2. Analysis of the X-ray Crystallographic Structure

The ORTEP drawing and atomic numbering are shown in Figure 2. The carbohydrate portion contains four chiral carbon atoms with the absolute configuration of the ring system (2*S*,3*S*,4*S*,5*R*) assigned on the basis of the known configuration for the starting D-galactose. The α -D-pyranose ring in crystalline D-tagatose-*N*-methylaniline exists in the $^5\text{C}_2$ chair conformation, with puckering parameters [19] $Q = 0.584(2)$ Å, $\theta = 1.7(2)^\circ$, and $\phi = 29(6)^\circ$. The related $^5\text{C}_2$ conformations of α -D-tagatopyranose [16], *N*-(1-deoxy- α -D-tagatopyranos-1-yl)-amino acids [8], tagatosamines [10,11], and 1-deoxy- α -D-tagatopyranose [17,18] were found as the major or only structures in both the solution equilibria and the in crystalline state (Table 1). These conformations are, thus, very close to the sugar ring structure in *N*-(1-deoxy- α -D-tagatopyranos-1-yl)-*N*-methylaniline.

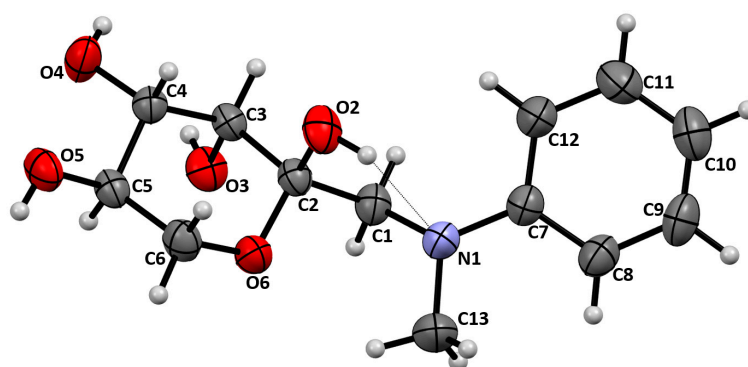


Figure 2. Atomic numbering and displacement ellipsoids at a 50% probability level for *N*-(1-deoxy- α -D-tagatopyranos-1-yl)-*N*-methylaniline. The intramolecular hydrogen bond is shown as a dotted line.

Bond distances and valence angles (Supplementary Table S4) in *N*-(1-deoxy- α -D-tagatopyranos-1-yl)-*N*-methylaniline compare well to the corresponding values found in α -D-tagatopyranose [16], 1-deoxy- α -D-tagatopyranose [17], 1-dibenzylamino-1-deoxy- α -D-tagatopyranose [10] and to average values for a number of crystalline pyranose structures [20]. The endocyclic torsions (Supplementary Table S5) do not differ significantly from the “standard” pyranoside torsions [20] with C–C–C–C(ring) at $\sim 55^\circ$, C–C–C–O(ring)- at $\sim 57.5^\circ$, and C–C–O–C- at $\sim 62.5^\circ$. The exocyclic angles around the ring bonds are close to the “ideal” 60° or 180° as well.

2.3. Analysis of Molecular Packing

The crystal packing and intermolecular hydrogen bonds in the crystalline D-tagatose-*N*-methylaniline are shown in Figure 3. The intermolecular H-bonding is localized in antiparallel layers oriented along the crystallographic *ac* plane. Within the layers, a system of intermolecular heteroatom contacts (4 out of 5, see Table 2) is dominated by hydroxyl groups which form a system of homodromic infinite chains running along the *b* axis. A simplified graphical representation of the network is shown in Figure 4. There is a pattern of linked infinite $C_3^3(6)$ and short $D_2^2(6)$ chains (a topological notation according to Bernstein et al. [21]). Aromatic rings with the shortest distances between their centroids ($5.410(2)$ Å) are located in planes with a small dihedral angle $16.7(1)^\circ$, but the rings are displaced by 3.5–4.4 Å relative to each other. Hence, π – π interactions do not appear to contribute to the crystal structure. Among candidates for the π – σ interactions, the shortest contact with the centroids is provided by the methyl group donors (Table 2).

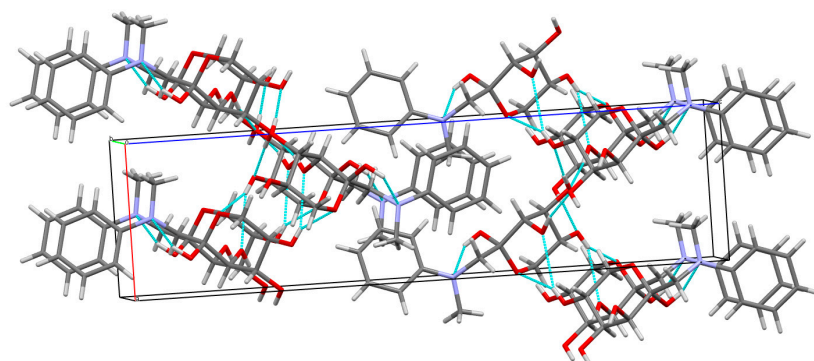
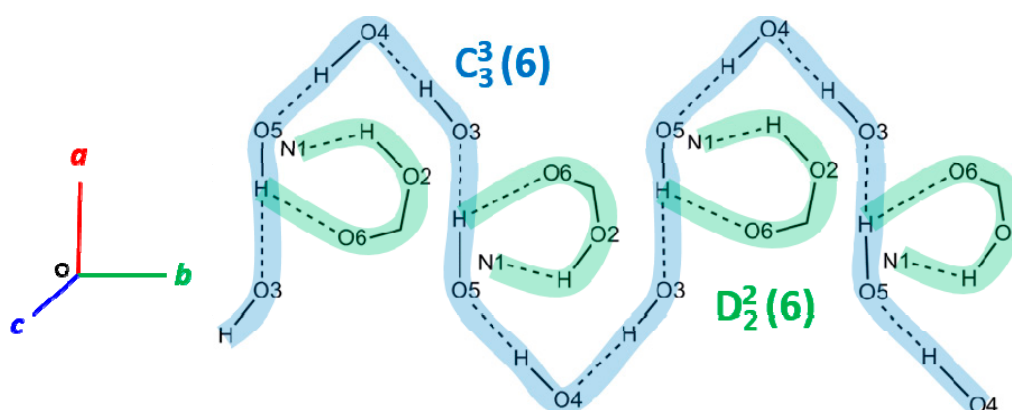


Figure 3. Crystal packing of *N*-(1-deoxy- α -D-tagatopyranos-1-yl)-*N*-methylaniline. Hydrogen bonds are shown as cyan dotted lines. Color coding for the crystallographic axes: red—*a*, green—*b*, blue—*c*.

Table 2. Hydrogen bonding geometry (\AA , $^\circ$) in the crystal structure of *N*-(1-deoxy- α -D-tagatopyranos-1-yl)-*N*-methylaniline.

Contact	D–H	H \cdots A	D \cdots A	D–H \cdots A	Symmetry Code ²
O2–H \cdots N1	0.79(2)	2.05(2)	2.816(1)	164(2)	intra
O3–H \cdots O4	0.88(3)	2.03(3)	2.878(1)	162(2)	$-1-x, -1/2+y, -1/2-z$
O4–H \cdots O5	0.75(3)	2.43(3)	3.114(1)	153(3)	$-1-x, -1/2+y, -1/2-z$
O5–H \cdots O3	0.75(3)	2.53(3)	2.885(1)	111(2)	$-2-x, 1/2+y, -1/2-z$
O5–H \cdots O6	0.83(3)	2.23(3)	3.058(1)	176(3)	$-2-x, 1/2+y, -1/2-z$
Suspected contacts					
C6–HA \cdots O2	0.97	2.44	2.771(2)	100	intra
C6–HB \cdots O3	0.97	2.50	3.289(2)	138	$-2-x, 1/2+y, -1/2-z$
C13–HB \cdots O6	0.96	2.39	3.060(3)	127	intra
C13–HA \cdots Cg1 ¹	0.96	2.93	3.859(3)	162	$-1/2+x, -1/2-y, -z$

¹ Cg1 refers to the benzene ring center of gravity. ² Symmetry code refers to the acceptor atoms.

**Figure 4.** Hydrogen bonding pattern in crystal structure of *N*-(1-deoxy- α -D-tagatopyranos-1-yl)-*N*-methylaniline.

2.4. Analysis of the Hirshfeld Surfaces

Taken together with our previous reports [13,15,22], this work completes a set of *N*-aryl derivatives of all four possible hexulosamines, including D-fructosamine, D-psicosamine, D-sorbosamine, and D-tagatosamine. There is one striking feature within this set that positions D-fructosamine apart from the rest of the hexulosamines. While the D-psicosamine, D-sorbosamine, and D-tagatosamine derivatives crystallize in the α -pyranose conformation, which is a dominant species in the amino sugar solutions, some *N*-aryl D-fructosamines tend to crystallize in a minor, acyclic conformation of the keto tautomer [13,15]. We have suggested previously that hydrophobic, non-polar interactions may play a significant role in the shaping of crystal packing forces for these molecules. One method to evaluate such interactions is to calculate and analyze the Hirshfeld surfaces, which are essentially weight functions that partition the crystal space between molecules contributing to the crystal structure [23].

A number of properties can be mapped over the Hirshfeld surface, including the electrostatic potential, topology, or interatomic contact distance functions. Figure 5 illustrates the latter, which we have calculated for the α -pyranose anomer of D-tagatose-*N*-methylaniline in crystal.

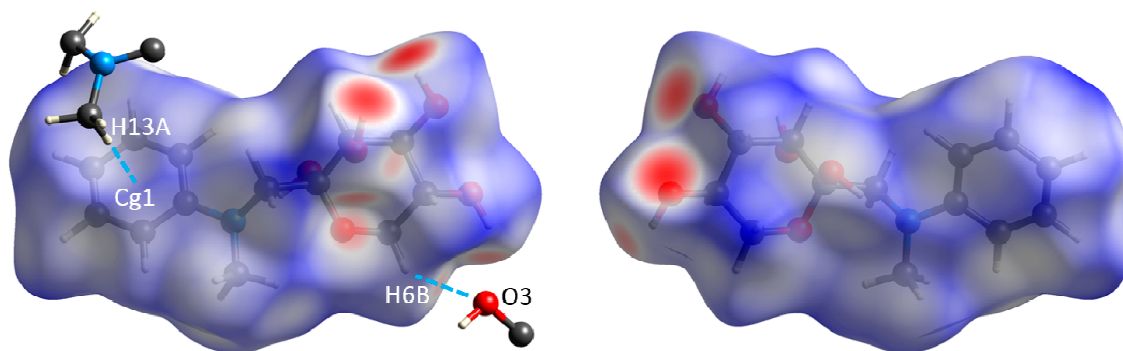


Figure 5. Views of the Hirshfeld surface for *N*-(1-deoxy- α -D-tagatopyranos-1-yl)-*N*-methylaniline, with the vdW-normalized contact distance function (d_{norm}) mapped in colors encoding intermolecular contacts, from closest (red) to the most distant (blue), in the range of -0.67 to 1.28 . Shown are molecular fragments involved in the C-H \cdots π interaction and the shortest C-H \cdots O contact.

To determine the relative contribution of hydrophilic and hydrophobic intermolecular contacts to the packing forces in crystalline *D*-tagatose-*N*-methylaniline, the contact distance functions were plotted as 2D graphs, the so called “fingerprint plots” [24]. As shown in Figure 6, there is a large (64%) contribution of non-polar H \cdots H contacts to the overall intermolecular interactions within the crystal. In addition, a significant proportion of the contacts (13%) are lowly polar C \cdots H contacts. Some of these include interactions between hydrogen atoms and aromatic ring centroids, as shown in Figure 5. Only a small proportion of intermolecular contacts (21%) are due to polar O \cdots H interactions, although not all of these qualify for conventional hydrogen bonds of the O \cdots H-O or N \cdots H-O types. A number of the contacts are of the O \cdots H-C type (exemplified in Table 2 and Figure 5), which are not directional and may have a rather circumstantial significance. These numbers are in agreement with structures of crystalline *N*-aryl *D*-sorbosamine and *D*-psicosamine derivatives [22] (62.2% for H \cdots H, 15% for C \cdots H, and 22% for O \cdots H contacts). In contrast, the acyclic conformation of crystal structures of *N*-aryl *D*-fructosamines [15] is characterized by significantly higher contributions from polar contacts (50–60% for H \cdots H, 8–13% for C \cdots H, and 23–32% for O \cdots H contacts) to the packing forces.

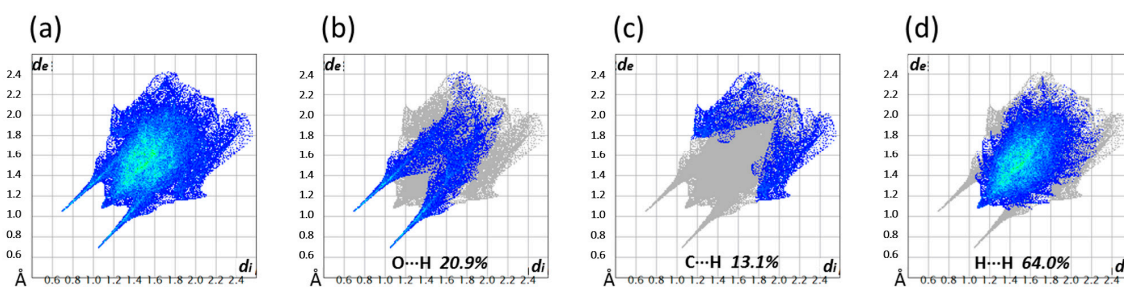


Figure 6. (a) The full two-dimensional plot for the d_e and d_i contact distance functions and those delineated for the specific contacts: (b) O \cdots H; (c) C \cdots H; (d) H \cdots H. The contributions of specific contacts to the intermolecular interactions are shown as percentages. Other contact type contributions not shown here: C \cdots O (2.0%) and C \cdots C (0.1%).

3. Materials and Methods

3.1. Synthesis of 1-Deoxy-1-(*N*-methylphenylamino)-*D*-Tagatose

The compound was prepared following a procedure [13] previously employed for the synthesis of fructosamines. A mixture of 3.6 g (20 mmol) of *D*-galactose, 2.4 g (22 mmol) of *N*-methylaniline and 0.55 mL (6.3 mmol) of 3-mercaptopropionic acid catalyst in 8 mL of isopropanol was stirred for

16 h in screw capped glass vials at 87 °C. The reaction progress was followed by TLC. The purification steps included an ion-exchange on Amberlite IRN-77 (H+), with 0.2 M NH₄OH in 50% EtOH as an eluent, and a flash filtration on a short silica column, using 5% MeOH in CH₂Cl₂ as an eluent. After evaporation of the eluates, crystallization of D-tagatose-*N*-methylaniline was aided by addition of acetone to the syrupy residue until turbidity was achieved. The crystalline material was filtered off, yielding 3.5 g (65%, based on starting D-galactose) off-white prisms, which provided monocrystals suitable for the X-ray diffraction studies. The major (α -pyranose anomer) peaks (ppm) in the ¹³C-NMR spectrum in 1:1 pyridine/D₂O (Supplementary Figures S1 and S2) were 153.46 (C-7); 131.10 (C-9, C-11); 119.12 (C-10); 115.53 (C-8, C-12); 101.57 (C-2); 74.87 (C-4); 74.21 (C-3); 69.22 (C-5); 65.20 (C-6); 61.95 (C-1); 42.06 (C-13). See Table 1 for minor peak assignments in the spectrum and Figure 1 for the solid-state ¹³C-NMR spectrum. The major signals (ppm) in the ¹H-NMR spectrum were 7.25 (t, 2H); 7.00 (d, 2H); 6.79 (t, 1H); 4.50 (m, 1H); 4.365 (d, 1H); 4.14 (m, 2H); 3.81 (d, 1H); 3.054 (s, 1H); 3.034 (s, 1H); 3.007 (s, 3H).

3.2. NMR

Solution ¹³C-NMR spectra (1:1 pyridine/D₂O) were recorded at 62.9 MHz and ¹H-NMR spectra (D₂O) and were obtained at 250.1 MHz using a Bruker ARX250 instrument (Bruker BioSpin, Billerica, MA, USA), with TSPS as an internal standard. The solid-state ¹³C-NMR experiments were done at 75.5 MHz with Bruker DRX300 wide bore NMR spectrometer (Bruker BioSpin, Billerica, MA, USA) equipped with a 7 mm solid CP-MAS probe. Zirconia rotors and KEL-F caps were used. The ¹³C CP-MAS-TOSS spectrum of solid glycine was measured first to check the performance of the spectrometer, and the chemical shift of the carbonyl peak was set to 176.03 ppm. The ¹³C CP-MAS-TOSS spectrum of the subsequent sample was acquired under the same conditions and referenced to this external standard. All samples were measured at room temperature with a spin rate of 5 kHz, 1 ms of contact pulse, and a 4 s repetition delay.

3.3. X-ray Diffraction Studies

The diffraction data were collected using the Enraf-Nonius CAD4 instrument (Bruker AXS, Madison, WI, USA). Crystal data and experimental details of the crystallographic studies are given in Supplementary Table S1. Briefly, the crystal data for C₁₃H₁₉NO₅ (M = 269.29 g/mol), which were used in all calculations, are as follows: orthorhombic, space group *P*2₁2₁2₁ (no. 19), *a* = 6.5757(10) Å, *b* = 7.7698(10) Å, *c* = 25.0403(10) Å, *V* = 1279.4(3) Å³, *Z* = 4, *T* = 295 K, μ (CuK α) = 0.899 mm⁻¹, *D*_{calc} = 1.398 g/cm³, 1559 reflections measured (7.0° ≤ 2 θ ≤ 149.1°), 1478 unique (*R*_{int} = 0.000, *R*_{sigma} = 0.029). The final *R*₁ was 0.0290 (*I* > 2 σ (*I*)) and *wR*₂ was 0.0762 (all data). The crystal structure was solved with the direct methods program, SHELXS-97 [25], and refined by full-matrix least squares techniques with the SHELXL2017 [26] suite of programs, with the help of X-Seed [27]. Data were corrected for Lorentz and polarization effects and for absorption. Non-hydrogen atoms were refined with anisotropic thermal parameters. Hydroxyl hydrogen atoms were located in difference Fourier maps and were refined with fixed isotropic thermal parameters. The remaining H-atoms were placed at calculated positions and included in the refinement using a riding model. As a result of the unrealistic value obtained for the Flack absolute structure parameter, 0.0(2), the absolute configuration of the ring system (2*S*,3*S*,4*S*,5*R*) was assigned on the basis of the known configuration for starting D-galactose. The structure was visualized with Mercury [28].

3.4. Molecular Hirshfeld Surfaces Calculations

The Hirshfeld surfaces analyses were performed and plotted using CrystalExplorer v.17.5 software (University of Western Australia, <http://hirshfeldsurface.net>) [23].

4. Conclusions

In this work, we employed a classic Amadori rearrangement method for synthesis of a glycoaminoconjugate. Despite being nearly a century old, this simple protocol was useful in the preparation of a rare amino sugar structure, D-tagatosamine, from a readily available carbohydrate source, D-galactose.

D-Tagatose-*N*-methylaniline is conformationally unstable in solution and exists in at least five anomeric/tautomeric forms, the most abundant of which is α -pyranose. This anomer represents a single conformation of D-tagatose-*N*-methylaniline in the crystalline state. The crystal structure consists of interchanging “carbohydrate” and “aromatic” layers. The carbohydrate portions of the molecules participate in an extensive system of intermolecular hydrogen bonding, whereas the non-polar contacts provide a major contribution to the overall packing forces in the crystal.

Supplementary Materials: The following are available online, Figure S1: ^{13}C -NMR spectrum of D-tagatose-*N*-methylaniline in 1:1 pyridine/D₂O; Figure S2: An expanded carbohydrate region of ^{13}C -NMR spectrum of D-tagatose-*N*-methylaniline in 1:1 pyridine/D₂O showing resolution of signals for the anomeric/tautomeric forms; Table S1: Crystal data, data collection and structure refinement details; Table S2: Atomic Parameters x , y , z and B or Beq ; Table S3: List of $u(i,j)$ or U values $\times 100$; Table S4: Bond distances (\AA) and angles ($^\circ$); Table S5: Torsion angles ($^\circ$); checkCIF/PLATON report. The complete crystallographic data for the structural analysis have been deposited with the Cambridge Crystallographic Data Centre, CCDC # 831970. Copies of this information may be obtained free of charge from the Director, Cambridge Crystallographic Data Centre, 12 Union Road, Cambridge, CB2 1EZ, UK. (Fax: +44-1223-336033, e-mail: deposit@ccdc.cam.ac.uk or via: www.ccdc.cam.ac.uk).

Author Contributions: V.V.M. and T.P.M. conceived and designed the experiments; V.V.M. synthesized the compound; C.L.B. collected the diffraction data; V.V.M. and C.L.B. analyzed the data; V.V.M. wrote the paper. All authors read and approved the final manuscript.

Funding: This work was funded, in part, by the University of Missouri Agriculture Experiment Station Chemical Laboratories and the National Institute of Food and Agriculture, grant No. MO-HABC0002.

Acknowledgments: The authors thank Wei G. Wycoff for help in the NMR experiments.

Conflicts of Interest: The authors declare no conflict of interest.

References

1. Deeth, H.C.; Lewis, M.J. *High Temperature Processing of Milk and Milk Products*; Wiley: Chichester, UK, 2017; 584p.
2. Moeller, A.B. Chemical changes in ultra heat treated milk during storage. *Prog. Food Nutr. Sci.* **1981**, *5*, 357–368.
3. Van Boekel, M.A.J.S. Effect of heating on Maillard reactions in milk. *Food Chem.* **1998**, *62*, 403–414. [[CrossRef](#)]
4. Nursten, H. *The Maillard Reaction: Chemistry, Biochemistry and Implications*; The Royal Society of Chemistry: Cambridge, UK, 2005; 214p.
5. Friedman, M. Biological effects of Maillard browning products that may affect acrylamide safety in food: Biological effects of Maillard products. *Adv. Exp. Med. Biol.* **2005**, *561*, 135–156. [[PubMed](#)]
6. Denisevitch, T.V.; Semyonova-Kobzar, R.A.; Glinsky, V.V.; Mosin, V.V. The influence of synthetic aminoglycoconjugates on the aggregation ability and metastatic potential of tumor cells. *Exp. Oncol.* **1995**, *17*, 111–117.
7. Mossine, V.V.; Mawhinney, T.P. 1-Amino-1-deoxy-D-fructose (“fructosamine”) and its derivatives. *Adv. Carbohydr. Chem. Biochem.* **2010**, *64*, 291–402. [[PubMed](#)]
8. Kaufmann, M.; Meissner, P.M.; Pelke, D.; Mügge, C.; Kroh, L.W. Structure-reactivity relationship of Amadori rearrangement products compared to related ketoses. *Carbohydr. Res.* **2016**, *428*, 87–99. [[CrossRef](#)] [[PubMed](#)]
9. Corzo-Martinez, M.; Hernandez-Hernandez, O.; Villamiel, M.; Rastall, R.A.; Moreno, F.J. In vitro bifidogenic effect of Maillard-type milk protein-galactose conjugates on the human intestinal microbiota. *Int. Dairy J.* **2013**, *31*, 127–131. [[CrossRef](#)]
10. Harding, C.C.; Cowley, A.R.; Watkin, D.J.; Punzo, F.; Hotchkiss, D.; Fleet, G.W.J. 1-Amino-*N,N*-dibenzyl-1-deoxy- α -D-tagatopyranose methanol solvate. *Acta Crystallogr. E* **2005**, *61*, o1475–o1477. [[CrossRef](#)]

11. Pérez, S.; López-Castro, A.; Márquez, R. Structure of 1-benzyl(methyl)amino-1-deoxy- α -D-lyxo-hexulopyranose. *Acta Crystallogr. B* **1978**, *34*, 2341–2344. [[CrossRef](#)]
12. Mossine, V.V.; Glinsky, V.V.; Mawhinney, T.P. Antitumor effects of the early Maillard reaction products. In *The Maillard Reaction: Interface between Aging, Nutrition and Metabolism*; Thomas, M.C., Forbes, J., Eds.; Royal Society of Chemistry: Cambridge, UK, 2010; Volume 322, pp. 170–179.
13. Mossine, V.V.; Barnes, C.L.; Chance, D.L.; Mawhinney, T.P. Stabilization of the acyclic tautomer in reducing carbohydrates. *Angew. Chem. Int. Ed.* **2009**, *48*, 5517–5520. [[CrossRef](#)] [[PubMed](#)]
14. Ma, B.; Schaefer, H.F.; Allinger, N.L. Theoretical studies of the potential energy surfaces and compositions of the D-aldo- and D-ketohexoses. *J. Am. Chem. Soc.* **1998**, *120*, 3411–3422. [[CrossRef](#)]
15. Mossine, V.V.; Barnes, C.L.; Mawhinney, T.P. Crystal structure of the acyclic form of 1-deoxy-1-(N-methyl-p-methoxyphenylamino)-D-fructose. *Acta Crystallogr. E* **2018**, *74*, 127–132. [[CrossRef](#)]
16. Punzo, F.; Watkin, D.J.; Fleet, G.W.J. α -D-Tagatopyranose. *Acta Crystallogr. E* **2009**, *65*, o1393–o1394. [[CrossRef](#)] [[PubMed](#)]
17. Jones, N.A.; Jenkinson, S.F.; Soengas, R.; Izumori, K.; Fleet, G.W.J.; Watkin, D.J. The concomitant crystallization of two polymorphs of 1-deoxy- α -D-tagatose. *Acta Crystallogr. C* **2007**, *63*, o7–o10. [[CrossRef](#)] [[PubMed](#)]
18. Jones, N.A.; Jenkinson, S.F.; Soengas, R.; Fanefjord, M.; Wormald, M.R.; Dwek, R.A.; Kiran, G.P.; Devendar, R.; Takata, G.; Morimoto, K.; et al. Synthesis and NMR studies on the four diastereomeric 1-deoxy-D-keto-hexoses. *Tetrahedron Asymmetry* **2007**, *18*, 774–786. [[CrossRef](#)]
19. Cremer, D.; Pople, J.A. General definition of ring puckering coordinates. *J. Am. Chem. Soc.* **1975**, *97*, 1354–1358. [[CrossRef](#)]
20. Jeffrey, G.A.; Taylor, R. The application of molecular mechanics to the structures of carbohydrates. *J. Comput. Chem.* **1980**, *1*, 99–109. [[CrossRef](#)]
21. Bernstein, J.; Davis, R.E.; Shimoni, L.; Chang, N.-L. Patterns in hydrogen bonding: Functionality and graph set analysis in crystals. *Angew. Chem. Int. Ed. Engl.* **1995**, *34*, 1555–1573. [[CrossRef](#)]
22. Mossine, V.V.; Barnes, C.L.; Mawhinney, T.P. Molecular and crystal structure and the Hirshfeld surface analysis of 1-amino-1-deoxy- α -D-sorbopyranose and 1-amino-1-deoxy- α -D-psicopyranose (“D-sorbosamine” and “D-psicosamine”) derivatives. *J. Mol. Struct.* **2018**, *1160*, 73–79. [[CrossRef](#)]
23. Spackman, M.A.; Jayatilaka, D. Hirshfeld surface analysis. *CrystEngComm* **2009**, *11*, 19–32. [[CrossRef](#)]
24. Spackman, M.A.; McKinnon, J.J. Fingerprinting intermolecular interactions in molecular crystals. *CrystEngComm* **2002**, *4*, 378–392. [[CrossRef](#)]
25. Sheldrick, G.M. A short history of SHELX. *Acta Crystallogr. A* **2008**, *64*, 112–122. [[CrossRef](#)] [[PubMed](#)]
26. Sheldrick, G.M. Crystal structure refinement with SHELXL. *Acta Crystallogr. C* **2015**, *71*, 3–8. [[CrossRef](#)] [[PubMed](#)]
27. Barbour, L.J. X-seed—A software tool for supramolecular crystallography. *J. Supramol. Chem.* **2003**, *1*, 189–191. [[CrossRef](#)]
28. Macrae, C.F.; Bruno, I.J.; Chisholm, J.A.; Edgington, P.R.; McCabe, P.; Pidcock, E.; Rodriguez-Monge, L.; Taylor, R.; van de Streek, J.; Wood, P.A. Mercury CSD 2.0—New features for the visualization and investigation of crystal structures. *J. Appl. Crystallogr.* **2008**, *41*, 466–470. [[CrossRef](#)]

